Bandwidth Re-Configurable Wideband QAM-OFDM With Hybrid Integrated InP-Si_3N_4 Tunable Laser Source for Short-Reach Systems

Lakshmi Narayanan Venkatasubramani, *Member, IEEE*, Devika Dass, *Graduate Student Member, IEEE*, Colm Browning, *Senior Member, IEEE*, Chris GH Roeloffzen, *Member, IEEE*, Douwe Geuzebroek, and Liam Barry, *Senior Member, IEEE*

***Abstract*—High-capacity data transmission for intra/inter-data centre links has become necessary to accommodate the massive increase in data traffic. Data transmission needs to be reconfigured based on instantaneous demand or based on certain cyclical and predictive traffic patterns. In this work, we demonstrate a record high transmission rate of 200 Gbps/λ and 160 Gbps/λ with 40 GHz 32QAM and 40 GHz 16QAM OFDM signal (over C-band) using the wavelength-tunable InP-Si_3N_4 laser source from the integrated dual laser module for short-reach application. We also demonstrate the data transmission with bandwidth reconfigurability and flexible higher-order modulation allocation enabled by this laser source's low relative intensity noise (< -160 dB/Hz). We successfully show that the data transmission performance in back-to-back and over-fibre is within the standard FEC limits and goes beyond our previous works by leveraging wideband multi-carrier to achieve rates not yet shown before with this device.**

***Index Terms*—Fiber-optic communication systems, intensity modulation, direct detection, short-reach communication, photonic integrated circuits, silicon nitride, OFDM.**

I. Introduction

THE continuous evolution of technology and devices offering cloud-based services have induced a massive traffic flow through the data centre (DC) networks. This necessitates a shift towards using higher transmission capacity per lane by utilizing higher bandwidths and higher-order modulation formats in the DCs. The transmission can be optimized by reconfiguring the system based on instantaneous demand or based on certain cyclical and predictive traffic patterns. Moreover, integrated optical solutions that can reduce the power consumption and cost of the DCs need to be employed [1]. A simple intensity modulation direct-detection (IM-DD) based optical transmission system is considered a more advantageous and feasible solution because of its low construction cost and computational complexity.

Scaling capacities with single-carrier transmission entails stringent optimization at the transmitter, higher bit resolution samplers and a larger signal-to-noise ratio at the receiver. The use of multi-carrier transmission schemes like orthogonal frequency division multiplexing (OFDM) would be advantageous over pulse amplitude modulation (PAM) options as they exhibit flexible data assignment to subcarriers with software controllable subcarrier spacing, no change in the receiver side signal processing and allows the use of different flavours of OFDM that can optimise throughput or system complexity [2].

The choice of laser used for the transmission is also a critical factor that decides the performance limits. For IM-DD systems, relative intensity noise (RIN) is an important parameter that decides the performance limits when scaling the order of modulation [3]. In the past demonstrations, VCSELs with −140 dB/Hz RIN were deployed to transmit 100 Gbps 16QAM OFDM over a short distance of 100 m [4], and a single mode tunable DFB laser has been used for transmission of 178 Gbps OFDM over 2 km [5]. Authors in [6] have reported a 200 Gbps transmission over 1.6 km for a high receiver power of 7 dBm.

Previously, we have demonstrated the transmission of wideband 40 GHz 16QAM and 32 GHz 32QAM OFDM signals with a data rate of 160 Gbps using an InP-Si_3N_4 hybrid integrated dual laser module over a 1 km short-reach link [7]. Here, we extend the work to show a record-high data rate of 200 Gbps/λ with IM-DD multi-carrier signal using this dual laser module. We show the transmission reconfigurability of this system by demonstrating signal transmission at different bandwidths and using different modulation formats with just a simple subcarrier allocation in software. Higher-order modulation increases the transmission rate but requires stringent conditions of operations, such as large transmit power levels and higher signal-to-noise ratios (SNR). The sources of SNR degradation include noises from the electrical and optical amplifiers, various types of noises (quantization, jitter, effective number of bits- ENoB) from

Manuscript received 30 November 2022; revised 20 February 2023; accepted 13 March 2023. Date of publication 23 March 2023; date of current version 9 June 2023. This work was supported by Science Foundation Ireland under Grants 18/EPSRC/3591, 18/SIRG/5579, 12/RC/2276_P2, and 13/RC/2077_P2. *(Corresponding author: Lakshmi Narayanan Venkatasubramani.)*

Lakshmi Narayanan Venkatasubramani, Devika Dass, Colm Browning, and Liam Barry are with the Radio and Optical Communication Laboratory, School of Electronic Engineering, Dublin City University, 9 Dublin, Ireland (e-mail: lakshminarayanan.venkatasubramani@dcu.ie; devika.dass2@mail.dcu.ie; colm.browning@dcu.ie; liam.barry@dcu.ie).

Chris GH Roeloffzen and Douwe Geuzebroek are with LioniX International BV, 7521 AN Enschede, The Netherlands (e-mail: c.g.h.roeloffzen@lionix-int.com; d.h.geuzebroek@lionix-int.com).

Color versions of one or more figures in this article are available at https://doi.org/10.1109/JLT.2023.3261140.

Digital Object Identifier 10.1109/JLT.2023.3261140

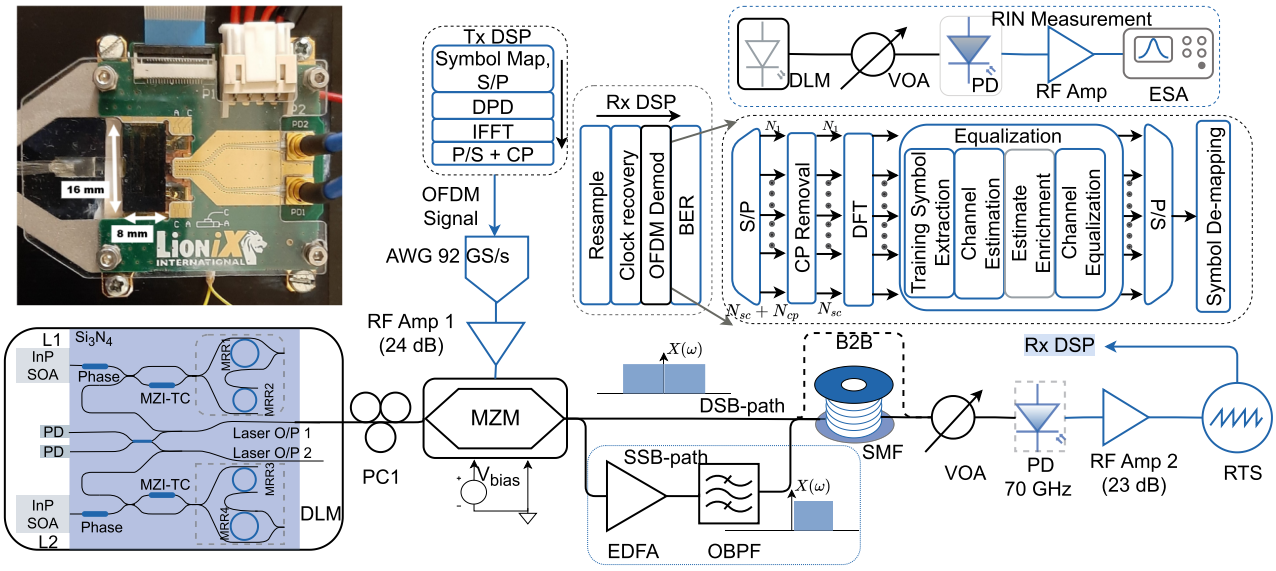

Fig. 1. Schematic of the experimental setup for the demonstration of wideband OFDM transmission using InP-Si$_3$N$_4$ laser. The setup for RIN measurement and the photograph of the DLM [3] are shown as insets.

the digital-to-analogue and analogue-to-digital converters and from the laser source itself. The fundamental SNR limitation from the optical source to the scale order of modulation is the laser RIN. Recently, the shaping and optimization of symbol constellations for transmission have been used to achieve maximum achievable information capacity and reduce the average energy [8]. In this work, we demonstrate the transmission of regular and shaped signal constellations to scale capacity while trying to operate at reduced transmit energy. The ability to transmit signals with higher cardinality is enabled by extremely low RIN (of < -160 dB/Hz) of the hybrid-integrated InP-Si$_3$N$_4$ tunable laser source. Being a silicon photonic (SiPh) integrated circuit, this device has a compact size, high yield, and potential for mass production and photonic integration with other SiPh components.

The overall structure of this article is as follows. In Section II, we briefly discuss the hybrid-integrated tunable laser and describe the experimental setup deployed using different modulation formats. Afterwards, in Section III, we present the results of the experiments performed with analysis and discussion on the same. Finally, we conclude the findings of this work in Section IV.

II. Laser Description and Experimental Setup

The simplified dual laser module (DLM) schematic is shown in Fig. 1 and consists of two on-chip lasers, L1 and L2, each having gain, phase and cavity sections, the 2×2 symmetric Mach-Zehnder Interferometer-based tunable couplers (MZI-TC) [8] and photodetectors (PDs). Each laser module is fabricated using an InP-based double reflective semiconductor optical amplifier (SOA) hybridly coupled to a Si$_3$N$_4$ feedback circuit. The feedback circuit contains two microring resonators MRRs in Vernier configuration. The on-chip micro-heaters (highlighted with blue in the simplified schematic of the laser) are linked to the phase section, the MRRs and the MZI-TC, enabling a thermo-optical control.

The InP-based SOA's right and left facets are coated with low and high reflective materials respectively, thereby assisting lasing phenomenon from the cavity. The free spectral range (FSR) of each Si$_3$N$_4$ feedback circuit with two MRRs is around 1.6 nm (200 GHz). The Si$_3$N$_4$ waveguides have an asymmetric double-stripe cross-section offering a low propagation loss of about 0.1 dB/cm, allowing the MRRs to reach extremely high Q-factors ranging from 20000 to 200000 [3], [9], [10].

We achieve wavelength tunability by optimizing micro-heaters' voltages associated with the feedback circuit and on-chip MZI-TC. A detailed description of this widely tunable and low-noise device is given in our previous work [3]. A photograph of the InP-Si$_3$N$_4$ hybrid integrated dual laser module used in this demonstration is shown in Fig. 1.

In this work, we have tuned one of the lasers of DLM over the C-band, and Fig. 2(a) shows the superimposed spectrum of test lines used, with side mode suppression ratio (SMSR) greater than 60 dB. For this work, we set the gain current to 170 mA and fine-tuned the voltages supplied to micro-heaters associated with the phase section, feedback circuit and on-chip tunable couplers. We then measure the RIN of one of the DLM output lines (1551.12 nm), as shown in Fig. 1. We detect the optical signal using a 30 GHz bandwidth photodetector (PD). The detected signal is then amplified using a 50 GHz RF amplifier and is fed to the electrical spectrum analyser (ESA, RS FSW50). The electrical spectrum is then used to compute the RIN as shown in Fig. 2(b) and has an extremely low value of ≈ -169 dB/Hz. The lower values of RIN compared to that in [3] are due to the increase in the current to the gain section of the laser. We now proceed with the data transmission using OFDM by using the output of the DLM.

In this work, we demonstrate the transmission using OFDM signals, where the complex domain symbols, derived from a

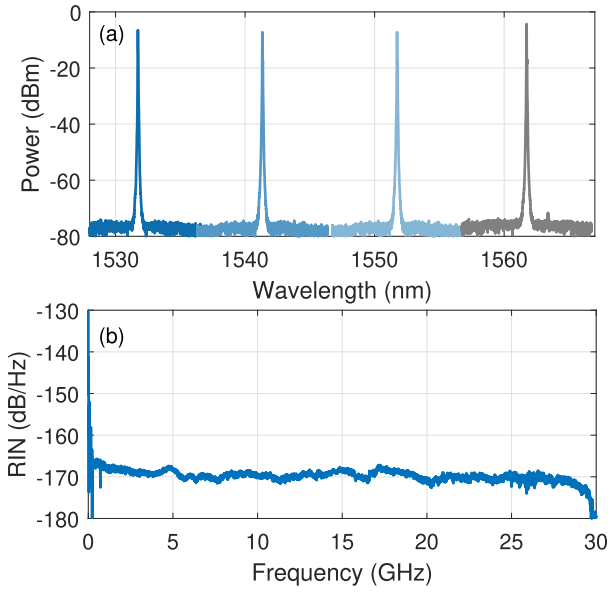

Fig. 2. (a) Superimposed spectra of the optical carrier used in this demonstration using the DLM. (b) The typical RIN of the DLM optical carrier at 1551.12 nm.

constellation set $\mathbf{Cs} = \{c_1, c_2, \ldots, c_M\}$ of order M, are modulated on each subcarrier. All the symbols in the set $\mathbf{Cs}$ here are considered to have a uniform probability of occurrence. The transmitted time domain OFDM signal $(x(k))$ is mathematically represented as

$$x(k) = \frac{1}{\sqrt{N_{sc}}} \sum_{m=0}^{N_{sc}-1} X_m e^{\left(\frac{j2\pi km}{N_{sc}}\right)}; \quad 0 < k < N_{sc} - 1, \quad (1)$$

where N_{sc} denotes the number of subcarriers of the OFDM symbol, and to generate a real OFDM signal, we employ Hermitian symmetry condition $X_{N_{sc}-l} = X^*{}_l, 0 < l < N_{sc}/2$ and $X \in \mathbf{Cs}$. One way to increase the data is by increasing the modulation order M of the symbols modulating each subcarrier. We employ different constellation symbols of different modulation orders and symbols with the same modulation order but having different constellation profiles like regular 32QAM and geometrically shaped 32QAM. The use of shaped constellations results in reduced average energy per symbol E_s and is calculated as follows [11]

$$E_s = \frac{1}{M} \sum_{j=0}^{M-1} \|c_j\|^2, \qquad c_j \in \mathbf{Cs}. \quad (2)$$

Fig. 3 shows the various modulation formats considered along with the values of E_s and the number of bits each symbol encodes (upper axis). In this work, the set of symbols for the constellation shaped (CS) 32QAM is derived from $\mathbf{Cs} = r_i e^{j((m+\frac{1}{2})\frac{\pi}{Nc_i})}$ with r and Nc the ring radius and the number of constellation symbols in the respective ring, and $\{r_i, Nc_i\}$ is $\{(1, 8); (2.5, 16); (3.5, 8)\}$ and $\{(1, 8); (2, 8); (3, 16)\}$ for CS-1 and CS-2 respectively. The set of CS-1 for 64QAM symbols is derived from $\mathbf{Cs} = r_i e^{j((m+\frac{1}{2})\frac{\pi}{16})}$ with $r = \{1; 2.5; 3.5; 4.75\}$.

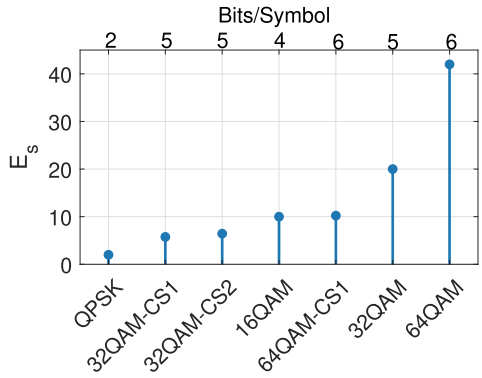

Fig. 3. Regular square and shaped modulation formats considered and their energy per symbol.

Fig. 1 shows the schematic of the experimental setup for transmitting wideband OFDM signals using the integrated hybrid InP-Si_3N_4 tunable laser module. We consider a pseudo-random bit sequence of order 17 and map the bits to symbols from the constellation considered. We then convert this serial data into $N_{sc}(= 256)$ parallel streams and appropriately load them on the data subcarriers. The desired bandwidth of the signal decides the number of data subcarriers used. We also introduce 5 zero subcarriers around DC to avoid signal-signal beat interference (SSBI) during direct detection. We then perform the inverse fast Fourier transform (iFFT) operation on all the subcarriers to convert it to the time domain. The parallel stream of time domain samples is then serialised, and a 16-sample cyclic prefix (CP) is added. We then perform amplitude clipping with a clipping ratio of 4 to reduce the time domain OFDM signal's peak-to-average power ratio (PAPR). We consider a baseband sampling rate of 92 GSa/s; hence, the subcarrier spacing (Δf) is ∼360 MHz. We then load 100 OFDM symbols (one frame) on the arbitrary waveform generator (AWG). An external cavity laser (ECL) and/or the DLM at a specific wavelength is used as an optical carrier and is fed to the Mach-Zender modulator (MZM, 40 GHz 3 dB bandwidth). The 92 GSa/s AWG generates the continuous-time electrical OFDM signal and gets amplified by an RF amplifier (24 dB gain). This amplified electrical signal drives the MZM to modulate the signal on the optical carrier to generate the double-sideband (DSB) optical signal. To study the effect of power fading, we also generate the single-sideband (SSB) signal by optically filtering out the amplified DSB signal generated previously. An optical amplifier is used in the SSB system to compensate for the insertion loss of the optical filter (XTM-50). We then consider the transmission of the DSB/SSB optical signal in back-to-back (B2B) and over single-mode fibre (SMF) (launch power of 5 dBm) configurations. We employ a variable optical attenuator (VOA) to change the received optical power of the signal before it is detected by a 70 GHz photodetector. The detected signal is then amplified by an RF amplifier (23 dB gain) and is captured using a real-time scope (RTS) (200 GSa/s). The digital samples are then further processed to evaluate the performance.

In the offline processing (as shown in Fig. 1 inset), the captured data is first normalized and then re-sampled to have exactly

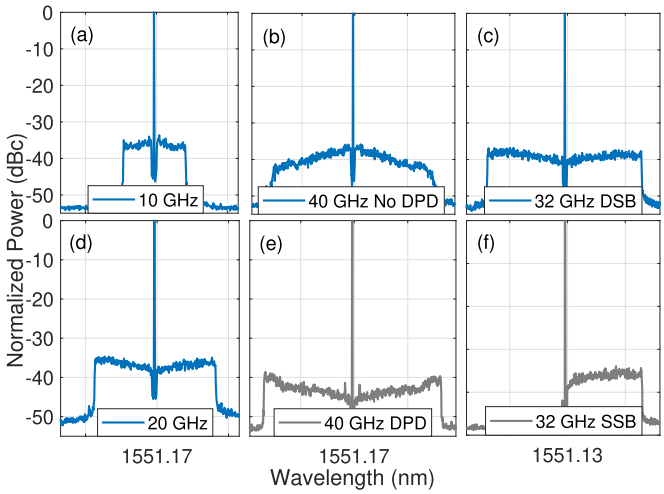

Fig. 4. Optical spectrum of the modulated signals with DPD (except for (b)) in different bandwidths and configurations. The bandwidth mentioned in the legend is a single-sided value and the x-axis grid lines are spaced at 0.2 nm.

1 sample per subcarrier. We perform frame synchronization based on standard correlation technique with the transmitted frame to locate the start of the frame in captured signal. We then remove CP from each OFDM symbol and convert the signal from time domain to frequency domain by performing an FFT operation. We estimate the channel response using the first five transmitted and received OFDM symbols. The estimates are enriched by employing the ensemble mean of intra-symbol spectral averaged channel estimates from the 5 training symbols. Next, the symbols were equalized using a single-tap frequency domain zero-forcing (ZF) equalizer to correct for the system imperfections. The equalized symbols are then de-mapped to bit sequences, and we evaluate the BER performance of the signal for each received optical power value.

Fig. 4 shows the optical spectrum of the modulated OFDM signal at different occupied bandwidths and for DSB and SSB configurations. The bandwidth mentioned in the legends of Fig. 4 is single-sided values corresponding to their electrical bandwidths. The figure also shows the 40 GHz DSB signal spectrum with and without digital pre-distortion (DPD). The DPD is applied to signals occupying a bandwidth greater than 10 GHz, and details of it are described in the following section.

III. Results and Discussion

Fig. 5(a) shows the BER performance of 10 GHz regular square 64QAM DSB-OFDM signal modulating the optical output from DLM (at 1551.12 nm) in B2B and 1 km SMF configurations, respectively. The plot also shows the reference hard-decision FEC (HD-FEC) line at a BER of 3.8×10^{-3} at 7% overhead. For B2B configuration, the BER performance of the signal is within the HD-FEC limit for received power >-1 dBm. The BER performance for transmission over 1 km SMF is within the HD-FEC limit for received power >-0.8 dBm. The total data rate of the transmission with regular 64QAM-OFDM is 60 Gbps.

Fig. 5(b) shows the BER performance of 20 GHz constellation-shaped CS-1 64QAM modulated DSB-OFDM signal with the optical source from DLM (at 1551.12 nm) in B2B and 1 km SMF configurations, respectively. The plot also shows the reference soft-decision FEC (SD-FEC) line at a BER of 2.2×10^{-2} at 20% overhead. We report a higher value of BER (and FEC limit) here because of the increased signal bandwidth and closed spacing of symbols in the shaped constellation. For B2B configuration, the BER performance of the signal attains the SD-FEC limit at -1.5 dBm received optical power.

The performance of the fibre transmission case is within the SD-FEC limit for received power >0 dBm. The total data rate of the transmission with CS-1 64QAM-OFDM is 120 Gbps. Fig. 6 shows the scatter plots of the successfully equalized regular 10 GHz 64QAM and 20 GHz CS-1 64QAM signals after 1 km SMF at a received power of 0 dBm, along with ideal reference constellation points marked with '$\times$' symbol.

Fig. 5(c) shows the BER performance of 20 GHz 32QAM modulated DSB-OFDM signal with two shaped constellation profiles (CS1 and CS2) with the optical carrier derived from DLM (at 1551.12 nm) in B2B and 1 km SMF configurations, respectively. The plot also shows the reference 7% overhead HD-FEC line. The data rate for both signals transmission is 100 Gbps. For B2B configuration, the BER performance of the signal attains the HD-FEC limit at received power of -1.5 dBm for CS-2 compared to -0.8 dBm for CS-1. We can observe an increased penalty of 0.6 dB in the case of CS-1 compared to the CS-2 constellation profile. This is because using CS-1 reduces the Euclidean distance between constellation points, with respect to CS-2, causing a relative degradation in BER for the same SNR. The performance of the 1 km fibre transmission case is within the HD-FEC limit for received powers above 0 dBm and 1 dBm for CS-2 and CS-1 signals, respectively. Fig. 7 shows the scatter plots of the successfully equalized 20 GHz CS-1 and CS-2 32QAM signals after 1 km SMF at a received power of 0 dBm.

We now evaluate the performance of OFDM signals modulated at higher bandwidth ($>$ 30 GHz). For systems employing larger bandwidths, the effective frequency response of all the system's components bounds the maximum achievable transmission capacity. An ideal system must have a flat frequency response across the signal bandwidth. However, in practice, the response is coloured since the usable bandwidth of the components is often extended beyond the 3 dB specified values rather than having a brick wall frequency response. Fig. 8(a) shows the normalized channel frequency response across the signal bandwidth estimated from the transmitted training symbols for 40 GHz and 32 GHz modulated OFDM signals. Compared to the centre subcarriers, the outermost subcarriers are attenuated by about 5 dB and 10 dB for 32 and 40 GHz signals. This frequency response affects the effective transmission capacity C since it effectively colours the SNR of the subcarriers as

$$C = \sum_{k=0}^{N_{sc}-1} log_2 \left(1 + \frac{S_{\Delta f_k}(f)}{N_{\Delta f_k}(f)} |H_{\Delta f_k}(f)|^2\right) \Delta f_k, \qquad (3)$$

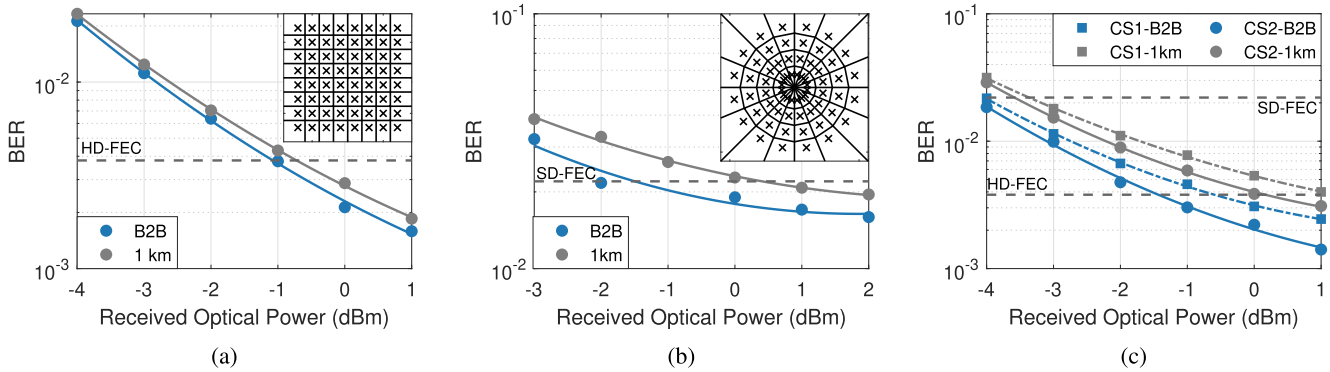

Fig. 5. BER performance of (a) 10 GHz regular square 64QAM-OFDM signal (b) 20 GHz shaped 64QAM-OFDM signal, and (c) 20 GHz shaped 32QAM-OFDM signals (CS-1 and CS-2) in B2B and after 1 km SMF transmission.

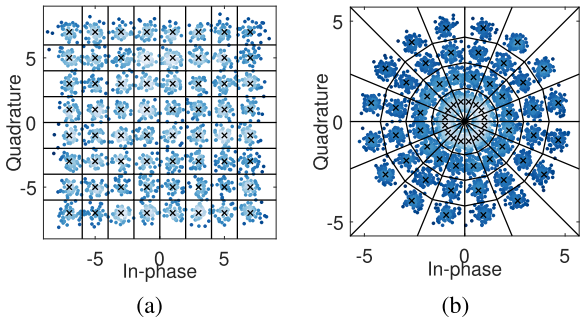

Fig. 6. Scatterplots of (a) 10 GHz regular and (b) 20 GHz CS-1 64QAM-OFDM signals after 1 km SMF transmission.

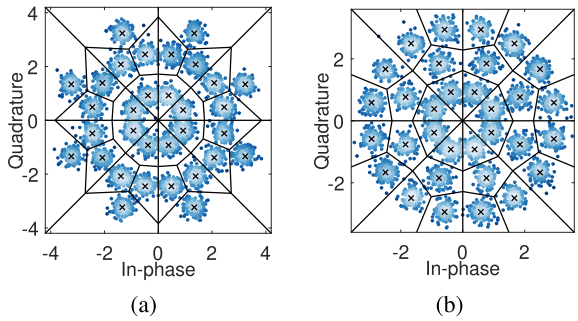

Fig. 7. Scatterplots of 20 GHz (a) CS-1 and (b) CS-2 shaped 32QAM-OFDM signals after 1 km SMF transmission.

where $S_{\Delta f_k}(f)$ is the PSD of the k^{th} subcarrier of the transmitted signal, $N_{\Delta f_k}(f)$ is the PSD of the noise and $H_{\Delta f_k}(f)$ is the channel response of the k^{th} subcarrier. To maximise the capacity and performance, we can either perform bit loading of the subcarriers by appropriately loading the symbols with a cardinality that best suits the channel response or perform power loading or digital pre-distortion by emphasising the higher frequency components to create a flat channel response. In this work, we perform digital pre-distortion by boosting the power of higher-frequency components. Fig. 8(b) shows the transmitter side electrical spectrum of the 32 and 40 GHz modulated OFDM signals with DPD.

Fig. 8(c) shows the BER performance of 32 GHz regular 32QAM signal performance with ECL and DLM (at different wavelengths) in B2B and 1 km SMF configurations, respectively. The plot also shows the reference SD-FEC lines at a BER of 2.2×10^{-2} and 3.8×10^{-2} at 20% and 25% overhead, respectively. For B2B configuration, the BER performance of the signal from ECL and at four wavelengths from DLM is within the 20% SD-FEC limit for received power >-4 dBm. For fibre transmission case, the performance is within the 25% SD-FEC limit for received power $>$-1 dBm.

We observe a penalty of about 3 dB for the fibre transmission case compared to B2B transmission, mainly due to the dispersive fading. Since the real OFDM signal has DSB and exhibits spectral conjugate symmetry, the power of the beat component upon direct detection varies as a function of the difference in phase accumulated of the corresponding subcarriers due to chromatic dispersion (CD). This variation in power as a function of fibre length (fading effect) can be mathematically described as the multiplication of real component of the fibre dispersion transfer function, $H_{\Re}(\omega)$, with the Fourier transform of detected signal [12], where

$$H_{\Re}(\omega) = \cos\left(\frac{1}{2}\beta_2\omega^2 L\right), \tag{4}$$

β_2 is the CD coefficient of the fibre at the laser's operating frequency, L is the fibre length, and ω is the angular frequency deviation from the laser's operating frequency. Fig. 9(a) shows an 8 dB power reduction due to the enhanced fading effect for the highest frequency subcarrier compared to the electrical spectrum of the received signal in B2B configuration. Although the information carrying bandwidth is 32 GHz, i.e. the electrical bandwidth, a large fading effect is observed for a short distance because the optical bandwidth spans to 64 GHz due to Hermitian symmetry. This fading effect reduces the SNR, especially at higher frequencies; hence, the performance is degraded.

Fig. 9(b) shows the BER performance of 40 GHz 16QAM signal with ECL and DLM in B2B and 1 km SMF configuration, respectively, and the performance is within 25% SD-FEC limit for received power >-3.5 dBm. The power penalty observed for fibre transmission compared to B2B results are again due to

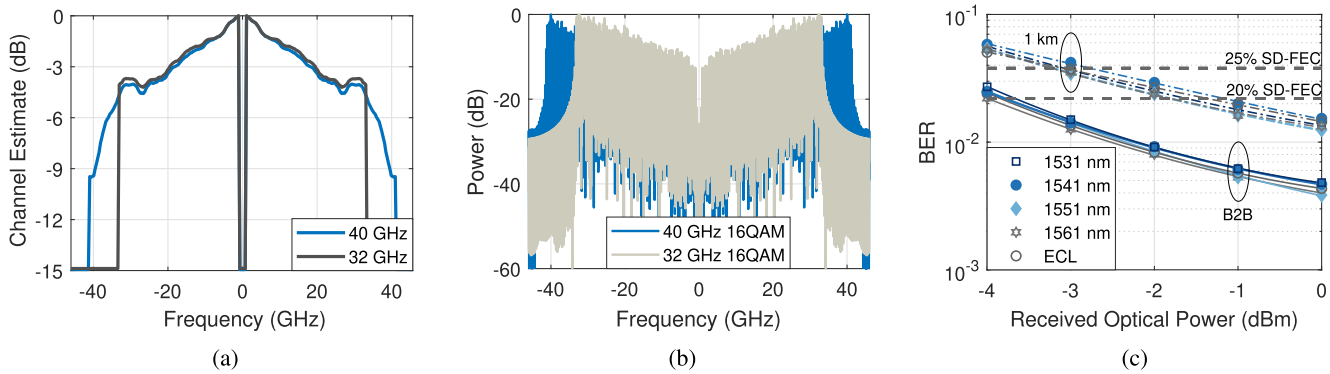

Fig. 8. (a) Channel estimates ($H(f)$) as a function of frequency. (b) Transmitter side DPD electrical spectrum of the 32 GHz and 40 GHz signal at the transmitter. (c) BER performance of 32 GHz 32QAM-OFDM signal in B2B and after 1 km SMF transmission, evaluated at various wavelengths across C-band.

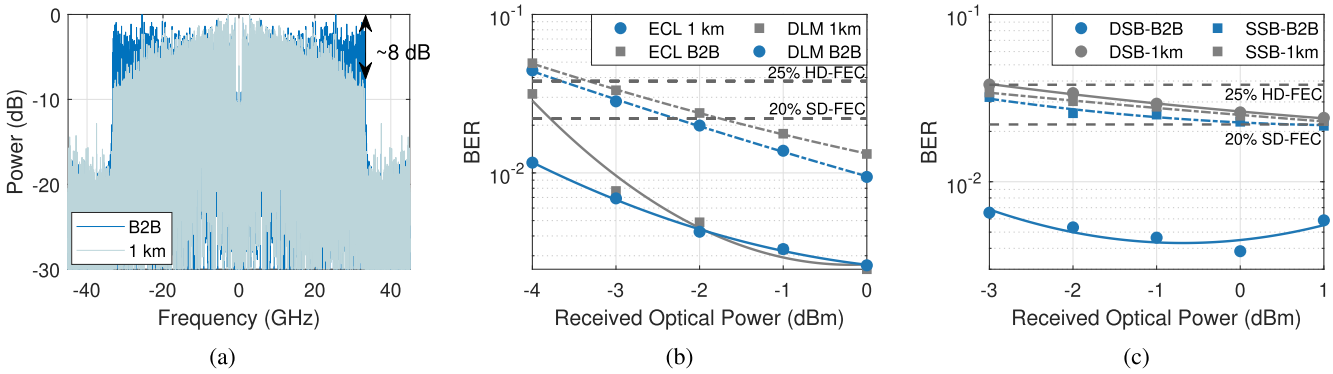

Fig. 9. (a) Effect of dispersive fading on the spectrum of the received 32 GHz signal after 1 km SMF transmission. BER performance of 40 GHz 16QAM-OFDM signal transmitted using (b) ECL and DLM sources in DSB configuration and (c) only DLM in both DSB and SSB configurations, in B2B and after 1 km SMF transmission.

the power fading effect. One way of avoiding the fading power effect is by employing SSB modulation, where only one side of the Hermitian symmetric spectrum is transmitted along with the carrier. This ensures that the power spectral density of the received signal remains intact to that of the transmitted signal and without being affected by $H_{\Re}(\omega)$. The generation of the SSB signal can be realized either by optical filtering of the generated DSB signal or by performing Hilbert transform to the DSB signal and modulating the in-phase (I) and quadrature (Q) components using an IQ modulator or a dual-drive MZM with appropriate bias conditions.

Due to the wideband nature of OFDM signal, we generate the optical SSB signal by employing an optical filter to filter out the carrier and one side of the spectrum, as shown in Fig. 1. Fig. 9(c) shows the BER performances of DSB and SSB 40 GHz 16QAM signals with DLM in B2B and 1 km SMF configurations, respectively. The plot also shows the reference SD-FEC lines at 20% and 25% overhead, respectively. For DSB configuration, the BER performance of signal in B2B and over fibre behaves as expected, with the BER of signal transmitted over fibre degraded due to fading. The BER performance of SSB signal in B2B and over 1 km SMF transmission is similar, demonstrating the absence of a power fading effect. The degradation in BER performance of SSB signal compared to DSB signal is because of the reduced SNR due to additional noise from the optical amplifier used in the SSB path to overcome the filter's insertion loss.

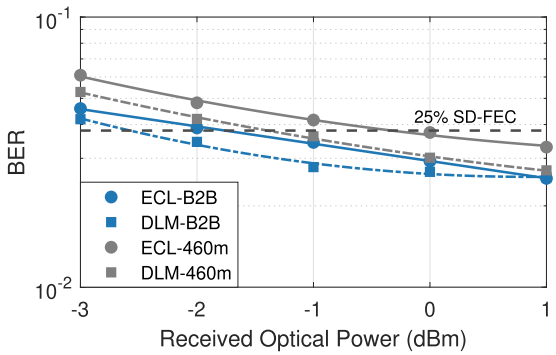

Fig. 10. BER performance of 200 Gbps real OFDM signal in B2B and with fibre transmission configurations.

We now discuss the BER performance of 200 Gbps/λ data transmission with 40 GHz regular 32QAM OFDM signal. Fig. 10 shows the BER performance of the 200 Gbps 32QAM-OFDM signal with ECL and DLM in B2B and 0.46 km SMF configuration, respectively. The performance is within 25% SD-FEC limit for received power $>$ 0 and -1 dBm for ECL

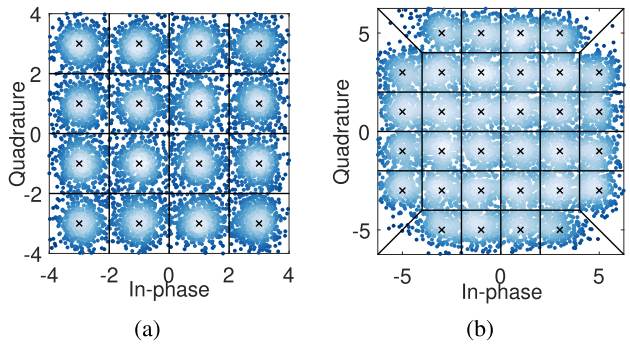

(a) (b)

Fig. 11. Scatterplots of 40 GHz (a) 16QAM and (b) 32QAM-OFDM signals after 1 and 0.46 km SMF transmission, respectively.

TABLE I
SUMMARY OF THE WIDEBAND OFDM SIGNAL TRANSMITTED WITH DLM AND THE PARAMETERS CONSIDERED

Data Bandwidth (GHz)	Modulation format	Data Rate (Gbps)
10	64QAM	60
20	CS-1 32QAM	100
20	CS-2 32QAM	100
20	CS-1 64QAM	120
32	32QAM	160
40 (Optical DSB)	16QAM	160
40 (Optical SSB)	16QAM	160
40	32QAM	200

and DLM, respectively. Fig. 11 shows the scatter plots of successfully equalized 40 GHz 16QAM (160 Gbps) and 40 GHz 32QAM (200 Gbps) signals after 1 km and 0.46 km SMF, respectively, at a received power of 0 dBm. The clear opening of the constellations is a visual measure of the performance, indicating a possibility of further BER reduction upon employing FEC. Some interesting conclusions are drawn from all the results. Firstly, the low relative intensity noise (~ -170 dB/Hz) of optical carrier from DLM source enabled the transmission of symbols of higher cardinality. The BER performance of the optical carriers from ECL and DLM are similar in most cases, whereas the performance of DLM is better in the 40 GHz higher-order QAM transmission case. This is because the wideband OFDM signal has a relatively lower SNR as available finite energy is spread across the bandwidth, and the low RIN from the DLM supports this transmission. Secondly, shaped constellations are advantageous since they have lower E_s than regular/square constellations. For example, CS-1 64QAM used here is $\sim 24\%$ energy efficient than regular 64QAM. However, very close packing of constellation symbols can result in degraded BER performance, as observed from CS-1 and CS-2 data transmission results. We can extend this to study and optimise the constellation shape to achieve the best possible power efficiency and transmission performance [11]. Thirdly, we have demonstrated almost similar performance of the transmission of wideband SSB and DSB OFDM signals, with the possibility of improving the performance of SSB signal by avoiding the optical amplifier. Employing SSB modulation not only reduces the effect of fading but also improves the reach and spectral efficiency, especially in multi-channel systems.

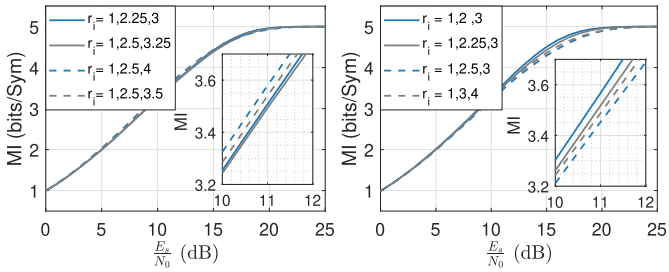

(a) CS-1 (b) CS-2

Fig. 12. Mutual information optimization for choosing the radii parameter for the 32QAM-OFDM with constellation shaping.

Table I shows the summary of the data transmission results deploying the optical output from DLM with various signal bandwidths and modulation formats and with the corresponding data rates. This discussed scheme can be employed in systems employing analogue multiplexers (AMUX) and higher bandwidth ($>$ 100 GHz) MZM to scale up the data rates [13]. In addition, a nonlinear equalizer, transmitter digital pre-distortion, and a simple single-tap equalizer could extend reach and enhance performance [14].

IV. CONCLUSION

Increasing capacity per lane in short-reach systems, especially in DC applications, has become crucial. With photonic integration and wide wavelength tuning capability, the InP-Si_3N_4 hybrid integrated DLM could potentially be deployed for simple optical-domain re-configurable wideband multi-channel systems. Integration of Si photonics-based modulators and lasers will result in low power-driven, cost-effective pluggable transmitters for high data rate intra/inter DC links [15]. The results presented here for 200 Gbps per wavelength channel with 40 GHz 32QAM-OFDM, 160 Gbps per wavelength channel (across C-band) with 32 GHz and 40 GHz OFDM signals, and 10 GHz/20 GHz regular and shaped constellation of 32QAM and 64QAM demonstrate the significant potential of re-configurable wideband OFDM systems employing tunable and low RIN laser sources for energy-efficient high capacity short reach systems.

APPENDIX

The use of shaped constellations of higher cardinality QAM was to exploit the low RIN of the DLM. To choose the desired constellation, we performed a simple optimization process by varying the radius parameter for the shaped constellation set and observed the mutual information (MI) at various signal-to-noise ratios (SNR) as shown in Fig. 12. From Fig. 4(d), we estimated an average SNR of the modulated signal of about 11 dB across all the modulated subcarriers. In the simulation, we evaluated the performance at this 11 dB SNR for both the shaped constellation configurations and the zoomed-in plots are shown as insets in Fig. 12(a) and (b) respectively. We observe that the MI performance of sets with larger radius spacing in CS-1 outperforms the ones with lower spacing and we chose the set $r_i = \{1\,2.5\,3.5\}$ since it has optimum performance and has lower symbol energy.

Similarly, we observe that the MI performance of the constellation sets of CS-2 having a radial spacing of 1 and 1.5 units is better compared to other configurations. Hence, we chose the set $r_i = \{1\,2\,3\}$ considering optimum performance and lower symbol energy.

We also checked in the experiment the performance of these constellation sets at a received power of 1 dBm and the performance corroborated with the simulation. The relatively lower value of the MI observed at this SNR translates to employing an FEC with a larger overhead to achieve an arbitrarily low BER after performing the error correction. Even though we have performed only a preliminary optimisation for the constellation radius, there is further scope to investigate the possible optimised geometric configuration [16], [17].

ACKNOWLEDGMENT

The authors would like to acknowledge fruitful discussions with Amol Delmade.

REFERENCES

[1] B. Wohlfeil, G. R. Mehrpoor, A. Dochhan, D. Rafique, M. Eiselt, and J.-P. Elbers, "Photonic integrated circuits for data center interconnects," in *Proc. Photon. Switching Comput.*, 2018, pp. 1–3.

[2] X. Zhang, Z. Babar, P. Petropoulos, H. Haas, and L. Hanzo, "The evolution of optical OFDM," *IEEE Commun. Surv. Tut.*, vol. 23, no. 3, pp. 1430–1457, thirdquarter 2021.

[3] D. Dass et al., "28 GBd PAM-8 transmission over a 100 nm range using an InP-Si$_3$N$_4$ based integrated dual tunable laser module," *Opt. Exp.*, vol. 29, no. 11, pp. 16563–16571, 2021.

[4] C.-Y. Huang et al., "Comparison of high-speed PAM4 and QAM-OFDM data transmission using single-mode VCSEL in OM5 and OM4 MMF links," *IEEE J. Sel. Topics Quantum Electron.*, vol. 26, no. 4, pp. 1–10, Jul./Aug. 2020.

[5] C. Kottke, C. Schmidt, K. Habel, and V. Jungnickel, "178 Gb/s short-range optical transmission based on OFDM, electrical up-conversion and signal combining," in *Proc. 42nd Eur. Conf. Opt. Commun.*, 2016, pp. 1–3.

[6] X. Pang et al., "200 Gbps/lane IM/DD technologies for short reach optical interconnects," *J. Lightw. Technol.*, vol. 38, no. 2, pp. 492–503, Jan. 2020.

[7] L. N. Venkatasubramani, D. Dass, A. Delmade, C. G. Roeloffzen, D. Geuzebroek, and L. Barry, "Wideband QAM-OFDM with hybrid integrated InP-Si$_3$N$_4$ tunable laser source for short-reach systems," in *Proc. Eur. Conf. Opt. Commun.*, 2022, pp. 1–4.

[8] C. G. Roeloffzen et al., "Silicon nitride microwave photonic circuits," *Opt. Exp.*, vol. 21, no. 19, pp. 22937–22961, 2013.

[9] C. G. Roeloffzen et al., "Low-loss Si$_3$N$_4$ triplex optical waveguides: Technology and applications overview," *IEEE J. Sel. Topics Quantum Electron.*, vol. 24, no. 4, pp. 1–21, Jul./Aug. 2018.

[10] Y. Fan et al., "290 Hz intrinsic linewidth from an integrated optical chip-based widely tunable InP-Si$_3$N$_4$ hybrid laser," in *Proc. Conf. Lasers Electro- Opt.*, 2017, pp. 1–2.

[11] E. Agrell and M. Karlsson, "Power-efficient modulation formats in coherent transmission systems," *J. Lightw. Technol.*, vol. 27, no. 22, pp. 5115–5126, Nov. 2009.

[12] M. Chagnon, "Optical communications for short reach," *J. Lightw. Technol.*, vol. 37, no. 8, pp. 1779–1797, Apr. 2019.

[13] H. Yamazaki et al., "IMDD transmission at net data rate of 333 Gb/s using over- 100-GHz-bandwidthanalog multiplexer and Mach–Zehnder modulator," *J. Lightw. Technol.*, vol. 37, no. 8, pp. 1772–1778, Apr. 2019.

[14] J. Shi, Y. Zhou, Y. Xu, J. Zhang, J. Yu, and N. Chi, "200-Gbps DFT-S OFDM using DD-MZM-based twin-SSB with a MIMO-volterra equalizer," *IEEE Photon. Technol. Lett.*, vol. 29, no. 14, pp. 1183–1186, Jul. 2017.

[15] E. El-Fiky et al., "A 4-lane 400 Gb/s silicon photonic transceiver for intra-datacenter optical interconnects," in *Proc. Opt. Fiber Commun. Conf.*, 2019, pp. 1–3.

[16] A. Mirani, E. Agrell, and M. Karlsson, "Low-complexity geometric shaping," *J. Lightw. Technol.*, vol. 39, no. 2, pp. 363–371, Jan. 2020.

[17] E. Sillekens, G. Liga, D. Lavery, P. Bayvel, and R. I. Killey, "High-cardinality geometrical constellation shaping for the nonlinear fibre channel," *J. Lightw. Technol.*, vol. 40, no. 19, pp. 6374–6387, Oct. 2022.